Optical characterization of the nematic lyotropic chromonic liquid crystals: Light absorption, birefringence, and scalar order parameter

Yu. A. Nastishin,[1,3] H. Liu,[2] T. Schneider,[2] V. Nazarenko,[4] R. Vasyuta,[4] S. V. Shiyanovskii,[1,2] and O. D. Lavrentovich[1,2,*]
[1]*Liquid Crystal Institute, Kent State University, Kent, Ohio 44242, USA*
[2]*Chemical Physics Interdisciplinary Program, Kent State University, Kent, Ohio 44242, USA*
[3]*Institute for Physical Optics, 23 Dragomanov street, Lviv, 79005 Ukraine*
[4]*Institute of Physics, NASU, prospekt Nauky 46, Kyiv 03039, Ukraine*
(Received 24 May 2005; published 25 October 2005)

We report on the optical properties of the nematic (*N*) phase formed by lyotropic chromonic liquid crystals (LCLCs) in well aligned planar samples. LCLCs belong to a broad class of materials formed by one-dimensional molecular self-assembly and are similar to other systems such as "living polymers" and "wormlike micelles." We study three water soluble LCLC forming materials: disodium chromoglycate, a derivative of indanthrone called Blue 27, and a derivative of perylene called Violet 20. The individual molecules have a planklike shape and assemble into rodlike aggregates that form the *N* phase once the concentration exceeds about 0.1*M*. The uniform surface alignment of the *N* phase is achieved by buffed polyimide layers. According to the light absorption anisotropy data, the molecular planes are on average perpendicular to the aggregate axes and thus to the nematic director. We determined the birefringence of these materials in the *N* and biphasic *N*-isotropic (*I*) regions and found it to be negative and significantly lower in the absolute value as compared to the birefringence of typical thermotropic low-molecular-weight nematic materials. In the absorbing materials Blue 27 and Violet 20, the wavelength dependence of birefringence is nonmonotonic because of the effect of anomalous dispersion near the absorption bands. We describe positive and negative tactoids formed as the nuclei of the new phase in the biphasic *N*-*I* region (which is wide in all three materials studied). Finally, we determined the scalar order parameter of the *N* phase of Blue 27 and found it to be relatively high, in the range 0.72–0.79, which puts the finding into the domain of general validity of the Onsager model. However, the observed temperature dependence of the scalar order parameter points to the importance of factors not accounted for in the athermal Onsager model, such as interaggregate interactions and the temperature dependence of the aggregate length.

DOI: 10.1103/PhysRevE.72.041711 PACS number(s): 61.30.St, 64.70.Md, 61.30.Gd, 61.30.Pq

I. INTRODUCTION

Lyotropic chromonic liquid crystals (LCLCs) represent a special class of lyotropic mesophases markedly different from the conventional amphiphilic mesogens [1–3]. Materials forming LCLCs are composed of planklike molecules with a polyaromatic central core and hydrophilic ionic (or hydrogen-bonding) groups at the periphery. The basic building block of LCLCs is a molecular stack in which the molecules are arranged in such a way that the ionic groups find themselves at the water-aggregate interface. In the nematic (*N*) phase, the columnar aggregates align parallel to each other but show no long-range positional correlations. The variety of possible geometries of aggregation is enriched by the fact that the molecular planes can adopt different orientations with respect to the axes of the aggregates. In the so-called *H* aggregates the molecular planes are nearly perpendicular to the columnar axis, i.e., the molecules are stacked on the top of each other, while in the so-called *J* aggregation the molecules are significantly shifted with respect to each other and thus their planes are strongly tilted towards the aggregate's axis [1–5]. The two types of aggregation differ noticeably in their spectroscopic properties, as the molecular interactions within the aggregates alter the absorption properties of the system as compared to the nonaggregated individual molecules [4–7]. Although it is plausible that the aggregates in LCLCs are formed by attraction between the central core of disklike or planklike molecules, there is no clear understanding of how exactly the molecules are arranged within the aggregates. Different models can be found in literature, including simple columns with one molecule in the cross section, columns with hollow center (a chimney type) and others [1–3]. It is also not clear whether aggregation in very diluted chromonic systems is characterized by a well-defined critical micellar concentration [1] that is so pronounced in the standard amphiphilic (surfactant-based) solutions in which self-assembly starts with a closed micelle formed by a well-defined number of molecules. As suggested by recent experiments on light scattering at the isotropic-nematic LCLC pretransitional fluctuations and shear viscosity measurements [8], the aggregation number and thus the length of LCLC aggregates increase when the temperature is reduced. Computer simulations demonstrate a similar effect when the concentration of LCLC molecules increases [9]; the effect is also apparent in light scattering and x-ray experiments with the LCLC material Sunset Yellow FCF studied recently by Horowitz *et al.* [10].

Despite the fact that the details of molecular arrangements in different LCLCs are still debated [1–3], the basic feature,

*Electronic address: odl@lci.kent.edu

namely, one-dimensional reversible self-assembly of their building blocks, makes it clear that the LCLCs should be very similar to many other important systems, namely, the "wormlike" micelles of surfactants, polyelectrolytes, and macromolecules of biological significance such as actin and tubulin [11]. The expected polydispersity of aggregates and the significant role of ionic groups make the LCLCs a valuable experimental system to test the recent theoretical models of one-dimensional self-assembly [12–15].

Because of the polyaromatic molecular core, many LCLC materials absorb light in the visible and near-infrared range [1,2]. This absorption is anisotropic, i.e., it depends strongly on the orientation of the LCLC molecules with respect to the polarization of light. Among the potential applications of LCLCs, the most actively pursued is the idea to use dried dye-based LCLCs films as light polarizing elements [16–26] in liquid crystal displays (LCDs), especially in flexible plastic LCDs [17–26]. In the late 1940s, Dryer and his colleagues proposed LCLCs as dichroic light-polarizing sheet materials [16]. LCLCs with no significant absorption in the visible part of spectrum could also be used as compensating films in LCDs [27]. Other emerging applications of LCLCs are in biological sensors as a medium to amplify the antibody-antigen binding and visualize the growth of immune complexes through director distortions [28] and in formation of nanostructured monolayers with long-range in-plane orientational order [29]. In the latter case, depositing the molecular monolayers of LCLCs onto a suitably charged substrate and using an atomic force microscope, one can directly visualize the bundles of LCLC rodlike molecular aggregates at nanometer scales [29].

The growing interest in LCLCs, both fundamental and applied, requires a detailed characterization of their optical properties. Progress in the field has been hindered by difficulties of uniform alignment of the director in the *N* phase. Without such an alignment, basic properties such as anisotropy of light absorption, birefringence, and the scalar order parameter are hard to determine. In most research articles, LCLCs are thus characterized spectroscopically as dyes, and not much attention is being paid to their anisotropic optical properties [1,3]. Recently, we developed a technique of uniform alignment of LCLCs based on buffed polyimide alignment layers and SiO layers [30]. In this paper, we take the advantage of this aligning technique and study in detail the optical anisotropic properties of three different nematic LCLCs, namely, disodium cromoglycate [DSCG, chemical formula $C_{23}H_{14}O_{11}Na_2$, Fig. 1(a)], which is transparent in the visible part of the spectrum and two absorbing dyes, 6,15-disulfonicacid-7,16-dichloro-6,15-dihydrodinaptho[2,3-*a*;2′,3′-h]phenazine-5,9,14,18-tetraone diammonium salt, called also Blue 27 [Fig. 1(b)], and 2,5-disulfonic acid diammonium salt-peryleno [3″,4″:3,4,5;10″,9″:3′,4′,5′] dipyridino [1,2-*a*:1′,2′-a′]bisbenzimidazol-6,11-diol, called also Violet 20 [Fig. 1(c)]. Blue 27 is a derivative of indanthrone and Violet 20 is a derivative of perylene. We determine the optical birefringence $\Delta n = n_e - n_o$ (n_e and n_o are the extraordinary and ordinary refractive indices, respectively) as a function of temperature T, weight concentration c, and wavelength λ, and the corresponding dependencies for the coefficients of absorption for Blue 27 and Violet 20. The absorption data are used to determine the scalar order parameter S for the *N* phase of Blue 27 and its temperature dependence. We also describe formation and structure of the tactoids observed in the biphasic region.

II. EXPERIMENTAL PART

A. Materials and sample preparation

All the solutions studied in our experiments were prepared using deionized water with initial resistivity of 18 MΩ cm.

1. DSCG

DSCG, also known as Cromolyn and Intal, was obtained from Spectrum Chemical Mfg. Corp. (Gardena, CA, CAS No. 15826-37-6). Although it is one of the most studied LCLCs [1,2,7,27,28] overall, the available data on Δn refer only to one concentration [27,28]. The DSCG molecule is formed by two rigid heterocycles connected by a flexible bridge that allows the molecule to assume many energetically similar conformations. One of the possible conformations of a free and isolated DSCG molecule, obtained through energy minimization in the Hartree-Fock approximation (PC SPARTAN PRO), is shown in Fig. 1(a); the two sodium cations at the opposite ends of the molecule appear blue in the color version online.

The liquid crystalline phases of DSCG, namely, the (uniaxial) *N* phase and a more highly ordered *M* phase, were first reported in the 1970s [31,32]. The *N* phase is formed by aggregates of stacked molecules. The aromatic cores of the molecules are on average perpendicular to the aggregate axis [33,34]. The detailed phase diagram of aqueous solutions of DSCG can be found in [1]. At room temperature (23 °C), the aqueous solution of DSCG is in the isotropic (*I*) phase for the (weight) concentration of DSCG, $c < 10$ wt %. In the range $10 < c < 12$ wt %, the solution demonstrates a wide biphasic region of coexisting *N* and *I* phases. The *N* phase is observed in the range $12 < c < 17$ wt %, another biphasic region with coexisting *N* and *M* phases at $17 < c < 21$ wt %, and the *M* phase at $21 < c < 35$ wt %. As demonstrated by x-ray diffraction [32], the molecular stacking distances along the axis of aggregates are about 0.34 nm, and the average distance between the aggregates scales approximately as $1/\sqrt{c}$ and decreases when the temperature is increased toward the isotropic phase. The scalar order parameter S has been estimated in deuterium NMR experiments by Goldfarb *et al.* [34]. S was found to be surprisingly high, ranging from 0.76 ± 0.08 to 0.97 ± 0.1 [34]; one of the possible reasons is that the studied range of concentrations spans through both the *N* and *M* phases.

For accurate measurements of S and other relevant parameters by optical means, the LCLCs need to be well aligned. Uniform alignment of LCLCs is hard to achieve. Ichimura and co-workers [35,36] reported that DSCG and the dye Direct Blue 67 can be aligned by irradiating a photosensitive polymer azo compound with linearly polarized light, when the material is doped with a nonionic surfactant. Our group

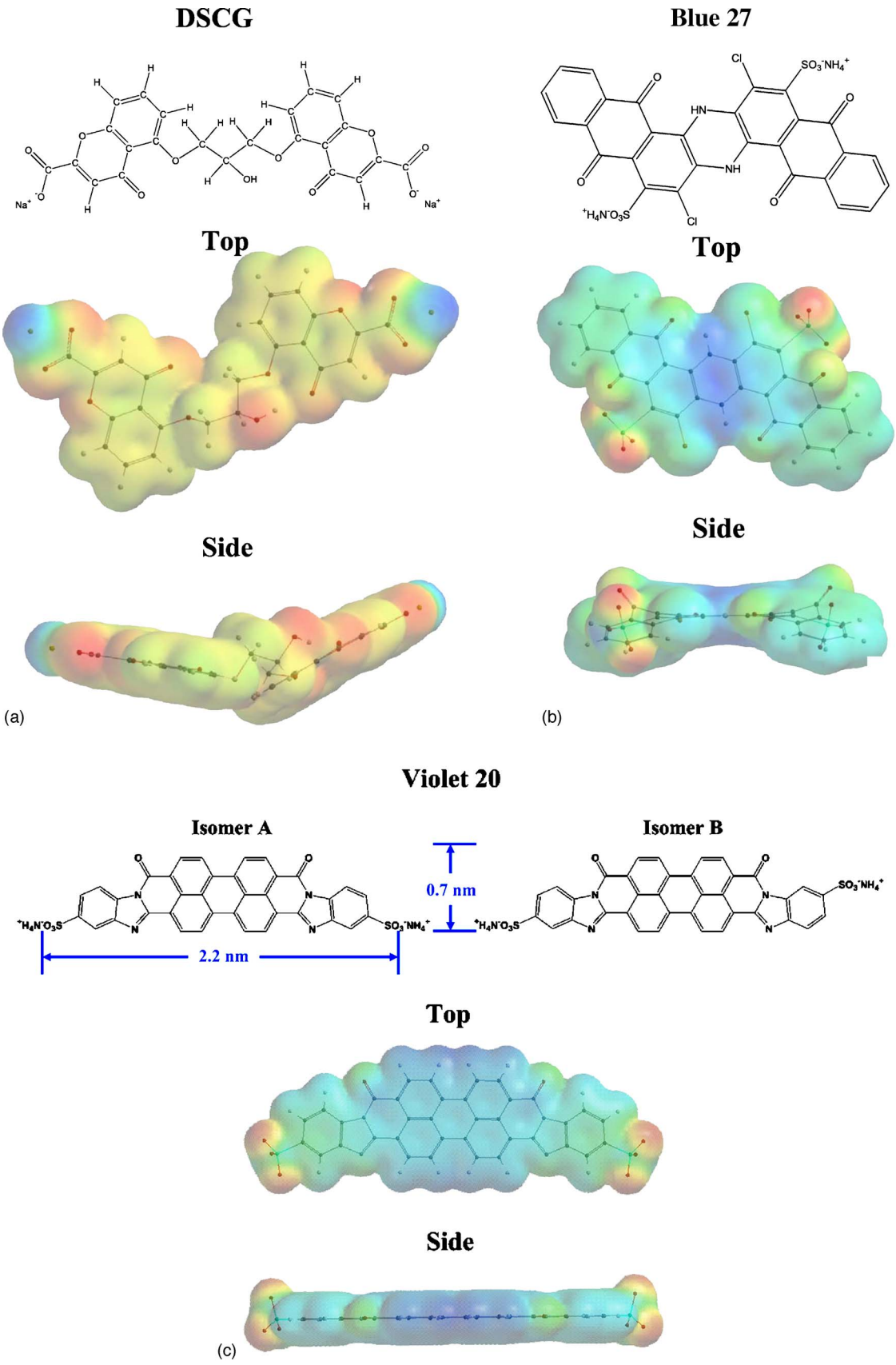

FIG. 1. (Color online) Structural formulas and molecular models for (a) DSCG, (b) Blue 27, and (c) isomers of Violet 20.

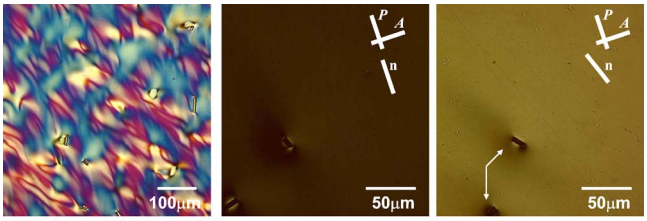

FIG. 2. (Color online) Polarizing microscope textures of DSCG (12.5 wt %) in two flat cells formed by (a) untreated glass plates, flow-induced alignment; (b),(c) glass plates with buffed polyimide SE-7511, as an aligning agent. (b) and (c) differ in the orientation of the average director with respect to the polarizer (*P*) and analyzer (*A*) directions; note the weak director distortions caused by the cylindrical spacers marked by arrows in part (c).

demonstrated that LCLCs could be aligned by certain buffed polyimide films and by obliquely deposited SiO layers; the technique does not require any surfactant (amphiphilic) additives [30]. In this work, we used spin-coated and buffed films of polyimide SE-7511 (Nissan Chemical Industries, Ltd.) to align the *N* phase of LCLCs in planar fashion, along a single direction in the plane of the bounding substrate determined by the direction of buffing. Glass substrates were washed in an ultrasonic bath of Alconox detergent and water for 10 min at 60 °C, removed, and dried. The polyimide SE-7511 Sunever, grade 7511L and the solvent Sunever, both from Nissan Chemical Industries, Ltd. (Japan) were mixed in the proportion 1:1. The solution was coated onto the glass substrates by a spincoater at 1500 rpm. The coating was dried at 100 °C for 2 min and then baked at 180 °C for 1 h. The polyimid-coated substrates were rubbed using an aluminum block covered with felt. The cells were assembled from pairs of substrates with rubbing directions being antiparallel to each other. The pretilt angle (measured between the director and the substrate) was less than 1°. Figure 2 demonstrates drastic difference in alignment quality between the regular glass cell with flow-induced alignment [Fig. 2(a)] and the cell with SE-7511 alignment layers [Figs. 2(b) and 2(c)].

The thickness of the gap between the glass plates in the LCLC cells was measured by the interference technique prior to the filling of the cells. The cells were filled by capillary flow assisted by negative pressure applied to one of the two open sides of the cell; the cell was promptly sealed after filling. The direction of flow and the pressure gradient were parallel to the buffing direction of the polyimide layers. To facilitate the capillary flow, the LCLC material was heated to the *I* phase (about 10 °C above the clearing point). The samples were also heated to about 10 °C above the *N-I* transition prior to each measurement, to mitigate the prehistory effects mentioned in Ref. [3]. The measurements were performed 2 h after cooling to the *N* phase.

2. Blue 27 and Violet 20

Blue 27 and Violet 20 were obtained from Optiva, Inc. (San Francisco, CA). Figures 1(b) and 1(c) show the corresponding molecular configurations as calculated by PC SPARTAN PRO using the semiempirical module and the

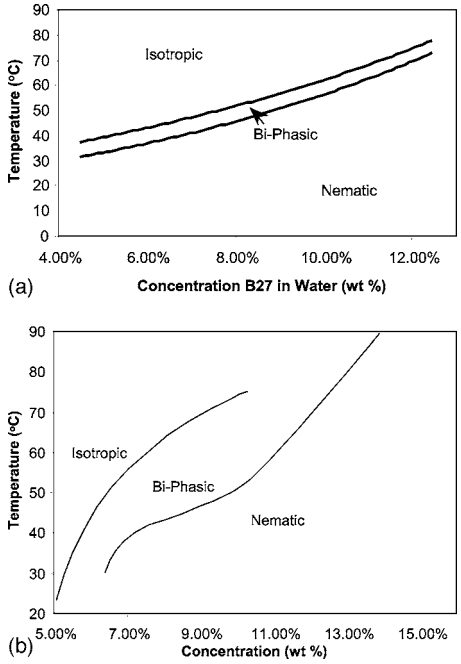

FIG. 3. Phase diagrams of aqueous solutions of Blue 27 and Violet 20.

Hartree-Fock approximation in the dissociated state (the two ammonium cations NH_4 have been omitted). The phase diagrams of aqueous solutions of Blue 27 and Violet 20 are shown in Fig. 3. The accuracy of the data on the transition temperatures is ±0.5 °C; the accuracy of the concentration data is better than ±0.1 wt %. Both phase diagrams feature relatively wide biphasic regions of the coexisting *N* and *I* phases, which is common also for DSCG. This broadening of the *N-I* coexisting region is generally attributed to the length polydispersity of the nematogenic building units [37–41].

The light absorption in aligned samples of both *N* materials is anisotropic with the maximum absorption for light polarized perpendicularly to the rubbing direction of the aligning layers, which is consistent with the *H* aggregation, as the absorption direction is in the plane of the molecule. Studies of molecular monolayers of both Violet 20 [29,42] and Blue 27 (Fig. 4) assembled by an electrostatic layer-by-layer deposition technique, also demonstrate that the absorption axis is perpendicular to the shear direction during deposition. Note, however, that the geometry of aggregates bounded by a charged substrate might be generally different from the geometry of aggregates in the bulk [29].

We performed x-ray scattering experiments (Cu $K\alpha$ radiation with $\lambda = 1.54$ Å) for the *N* sample formed by a 9.8 wt % aqueous solution of Blue 27 at room temperature. The solution was made to flow into a 3 mm Lindeman glass capillary using a pressure gradient. The director was parallel to the capillary axis. The x-ray diffraction pattern reveals a pronounced meridional peak that corresponds to ≈0.34 nm spacing along the director, Fig. 5. This feature is common for LCLC aggregates and is associated with the average distance between the molecular planes packed face-to-face along the aggregate's axis, see, for example, Refs. [1,10,32]. Interestingly, this distance of ≈0.34 nm is preserved even when the

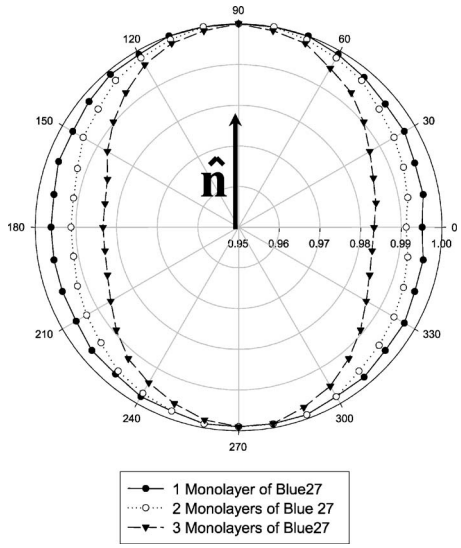

FIG. 4. Anisotropy of light absorption of dried films of Blue 27 at the light wavelength 650 nm formed by one, two, and three molecular monolayers. The monolayers were deposited onto the poly(diallyldimethylammonium chloride) substrate by the electrostatic layer-by-layer deposition technique from the *N* phase as described in [42].

sample is prepared as a dry film by shear aligning the N phase of Blue 27 onto a glass substrate and then letting it dry.

B. Measurement procedures and results

1. Positive and negative tactoids

One of the general features of the biphasic region in the studied LCLCs is the formation of positive or negative tactoids, Fig. 6, which are the inclusions of the *N* phase in the *I* phase or vice versa. These inclusions are of elongated cusped shape which is markedly different from the similar inclusions of nearly spherical shape observed in thermotropic nematics [43]. Polarizing microscopy reveals that the director is tangential to the *N-I* interface and forms two defects (boojums) at the cusped poles of the tactoids, Fig. 6. Similar tactoids were described by Bernal and Fankuchen for mesomorphic solutions of plant viruses [44]; tactoids can also form in concentrated actin gels [45]. Recently, there has been much interest as to the origins of tactoids [46–50]. Kaznacheev *et al.* explained the prolate shape as the result of competition between elastic energy of director distortions and the surface tension energy [46,48]. They observed tactoids in aqueous solutions of an inorganic lyotropic liquid crystal, vanadium pentoxide (V_2O_5). Prinsen and van der Schoot [47,49] came up with a more detailed model that predicts that the elongated tactoids in lyotropic systems should be generally free of the director twist, in contrast to thermotropic spherical nematic droplets in which the twist distortions often release splay and bend [51,52]. We compared polarizing microscopy textures of positive tactoids grown in a sealed 80-μm-wide circular capillary of 5 wt % solution of Violet 20 with a model in which the director field is along the circular arcs connecting the two poles; in other words, the director field follows the coordinate lines of the bipolar coordinate system with the origins at the poles [49]. The model textures of bipolar droplets were simulated using a computer algorithm described by Ondris-Crawford *et al.* [53]. As seen from Fig. 6(c), the model [49], in which the director follows the lines at the surfaces of revolutions of a circular arc about the main axis of the tactoid and thus displays only splay and bend but no twist, is in good agreement with the experimentally observed textures; see Ref. [54] for more details. As the director is strictly tangential to the *N-I* interface, the anchoring extrapolation length [43] for the *N-I* interface is much smaller than the size (40 μm) of the tactoid.

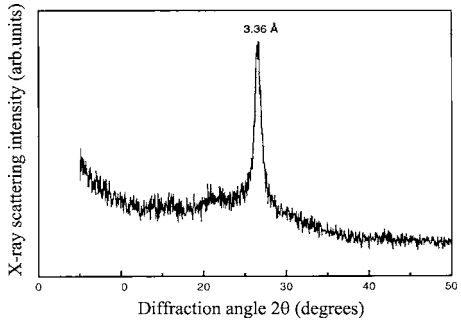

FIG. 5. Meridional scan of the x-ray scattering pattern for the *N* phase of Blue 27 at room temperature. The peak at 3.36 Å corresponds to the distance between the neighboring molecules in the stacks.

2. Optical spectra of isotropic solutions

We have measured the absorption spectra of DSCG (which absorbs mostly in the uv part of the spectrum [55]) and Blue 27 within the wide concentration range 10^{-4}–10^{-1} wt %, which corresponds to the *I* phase, to explore the possibility of abrupt formation of aggregates at some critical concentration. The spectra were recorded using Perkin Elmer, Lambda 18 spectrophotometer in the range 200–900 nm and quartz cells of thickness $d=75$ μm for high concentrations and $d=1$ cm for low concentrations. Figures 7 and 8 represent the data for the molar absorption coefficient $\epsilon=-\log_{10} t/dc_M$, where t is the optical transmission of the cell, c_M is the molar concentration measured in M =(mole/liter). The effect of solute on density is negligible in the range of studied concentrations, thus $c_M=10^3 c/M_{LCLC}$, where M_{LCLC} is the molecular mass of the corresponding chromonic material ($M_{B27}=685.8$, $M_{V20}=730.7$, and $M_{DSCG}=512.3$). The spectral dependencies of the molar absorption coefficient for DSCG [Fig. 7(a)] and Blue 27 [Fig. 8(a)] do not change their shape within the measured concentration range but the amplitudes of the absorption peaks increase when the concentration decreases. Usually, the concentration dependence of ϵ is absent or observed only for a relatively large c_M. In our case, the apparent concentration dependence of ϵ at low values of c_M can be related to at least three possible mechanisms. First, at small c_M, ϵ might depend on the average aggregate length and therefore, on c_M. Second, our experiments deal with total extinction to which not only absorption but also light scattering contributes; the latter

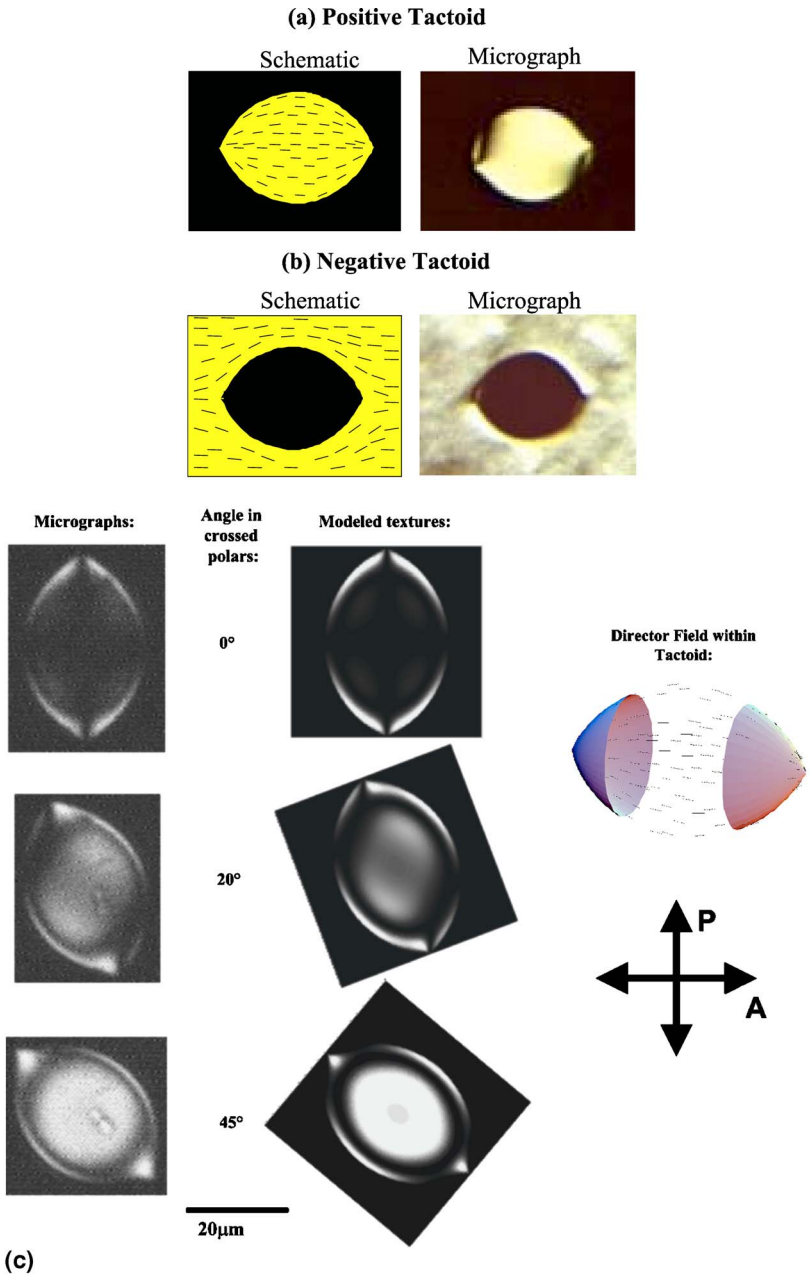

FIG. 6. (Color online) Polarizing microscopy textures of positive (a) and negative (b) tactoids formed in the biphasic region in a flat DSCG cell of thickness 20 μm. The length of the tactoids is about 40 μm. Part (c) compares the textures of a Violet 20 tactoid in the circular capillary of diameter 80 μm taken for different orientations with respect to the pair of crossed polarizers (left) to the computer-simulated textures (right) calculated using the model of Ref. [49] with the director bend and splay but no twist.

might have a different dependence on c_M. Third, the LCLC molecules can absorb at the walls of the cells, where their aggregation and absorption parameters would be different from that ones in the bulk; the difference would be more pronounced for very diluted solutions. The studies of these possibilities are in progress.

The spectra exhibit a complicated structure that is fitted with a set of several overlapping peaks of absorption. We assume a Gaussian form of each peak's contribution to the imaginary part of dielectric permittivity:

$$\mathrm{Im}\,\varepsilon(\nu) = \sum_i \frac{A_i}{\sqrt{2\pi}\Delta_i} \exp\left(-\frac{(\nu-\nu_i)^2}{2\Delta_i^2}\right), \qquad (1)$$

where $\nu=\lambda^{-1}$ is the wave number equal to the inverse light wavelength, A_i, ν_i, and Δ_i are the integral intensity, wave number corresponding to the maximum, and the width of the ith peak, respectively. The Gaussian shape of the peaks is usually attributed to their inhomogeneous broadening, caused by the fact that different excited molecules might be in different neighborhoods and thus their excitation energies

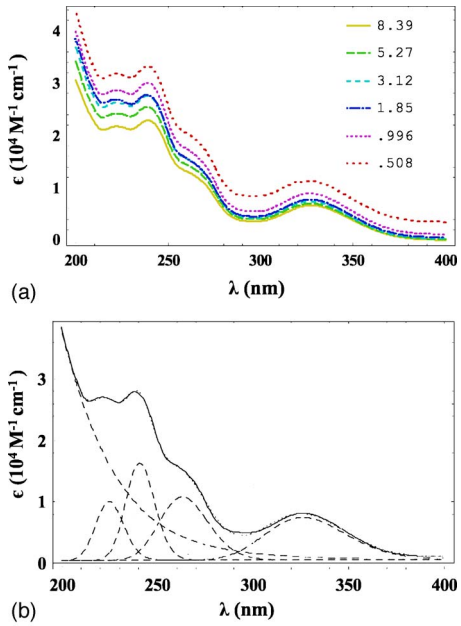

FIG. 7. (Color online) Spectra of the molar absorption coefficient ϵ for isotropic solutions of DSCG in water at $T=23\,^{\circ}\mathrm{C}$ in a quartz cell of thickness 75 μm for different molar concentrations shown in mM (a). Part (b) shows decomposition of the spectrum (solid line) for the concentration $c_M=1.85$ mM ($c=0.095$ wt %) into five Gaussian peaks (dashed lines). The reconstructed fitting curve (dotted line) practically coincides with the experimental data (solid line).

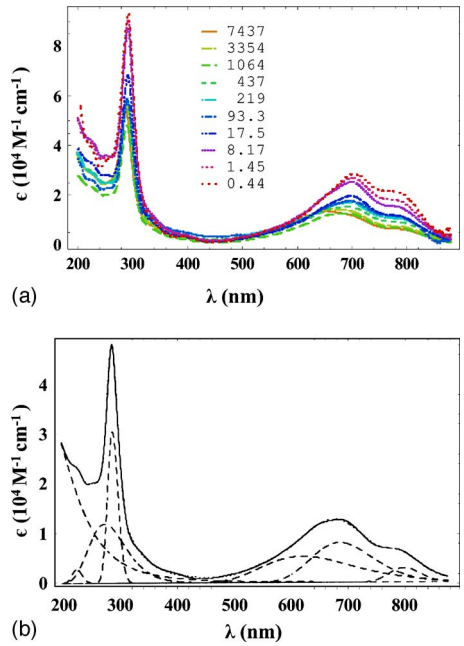

FIG. 8. (Color online) Spectra of the molar absorption coefficient ϵ of Blue 27 in water at $T=23\,^{\circ}\mathrm{C}$ for different molar concentrations shown in μM (a); the spectra were measured in a cell of thickness 75 μm with quartz substrates for higher molar concentrations ($c_M>50$ μM) and in a quartz cell with the light path $d=1$ cm for low concentrations. Part (b) shows decomposition of the spectrum (solid line) for the molar concentration $c_M=1064$ μM ($c=0.073$ wt %) into seven Gaussian peaks (dashed lines). The reconstructed fitting curve (dotted line) practically coincides with experimental data (solid line).

distribution might have a finite width. The assumption of Gaussian shape of the constituent peaks yields a good fit for the experimental spectra for both DSCG [Fig. 7(b)] and Blue 27 [Fig. 8(b)], while the same procedure with the assumption of Lorentzian shape does not fit the results (Lorentzian shape is associated with the finite lifetime of the excited states). The Gaussian fit demonstrates no measurable shift of the peaks throughout the whole concentration range from 10^{-4} to 10^{-1} wt %.

3. Birefringence and anisotropic absorption of N phase in planar samples

The measurements were performed on aligned samples of LCLCs, using a polarizing microscope Nikon OPTIPHOT2-POL, equipped with a computer-controlled Nikon microspectrophotometer comprised of a Photometry system P100S, Monochromator G70, and Photometer P102. The spectra were measured for a circular area of the sample (restricted by the microscope's pinhole) of diameter 10 μm. The sample was placed between a pair of parallel polarizers. To exclude the effects of reflection at the cell interfaces, the optical transmission t of the cells was calculated as a ratio of the transmitted light intensity I to the light intensity I_0 determined in the experiment with a cell that was identical to the test cell but filled with water instead of the LCLC, namely, I_0 was measured as the intensity of light passed through this water-filled cell.

a. DSCG: Birefringence. DSCG is transparent in the visible part of the spectrum. We determined its optical birefringence Δn by measuring the phase retardation $\Delta\varphi=2\pi\Delta nd/\lambda$ between the extraordinary and ordinary waves (Fig. 9). The director was oriented at 45° to the parallel polarizer and analyzer. Analyzing the transmission data for cells of different thickness and for different incident angles, we concluded that $\Delta\varphi$ in the cells with $d\leqslant 15$ μm was less than 2π in the studied range (400–700 nm). Using the data for normally incident light, Δn is calculated from the expression $t=\cos^2\Delta\varphi/2$. To illustrate the procedure, we show $t(\lambda)$ for three different concentrations, $c=12$, 15, and 17 wt % in Fig. 9(a). All the minima correspond to $\Delta\varphi=\pi$. As expected, the minima are shifted towards shorter wavelengths for lower concentrations indicating a smaller birefringence. The curves in Fig. 9(b) show dispersion of the birefringence as calculated from Fig. 9(a).

There are no anomalies in the observed wavelength range; Δn slowly decreases with λ and increases with c. We also measured Δn for tilted geometry: the sample was rotated around the rubbing direction by 30° with respect to the direction of incident light. We obtained the same Δn values within the accuracy range. This result implies that the N phase is optically uniaxial. We verified the negative sign of Δn in two separate experiments using a violet λ plate and a quartz wedge. The quartz wedge allows one to determine Δn independently, by compensating the birefringence of LCLC with the birefringence of the wedge. For example, the optical retardation of the 15-μm-thick DSCG cell can be compen-

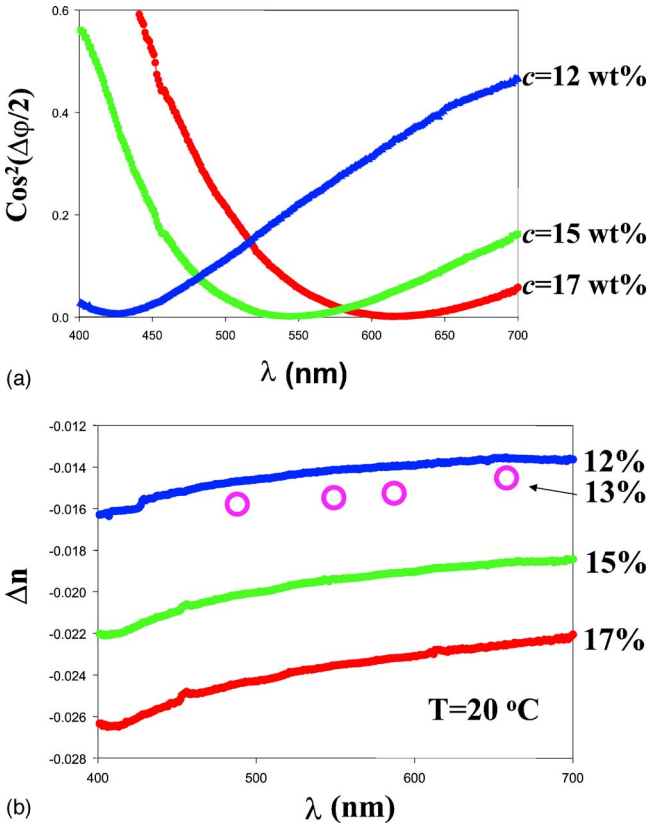

FIG. 9. (Color online) (a) Transmittance $t=\cos^2(\Delta\varphi/2)$ and (b) birefringence Δn of DSCG as measured for a planar cell at $t=20°$C for concentrations $c=12$ wt % ($d=13.5$ μm), 15 wt % ($d=14.0$ μm), and 17 wt % ($d=13.4$ μm); the open circles correspond to the Δn determined with a quartz wedge for $c=13$ wt %.

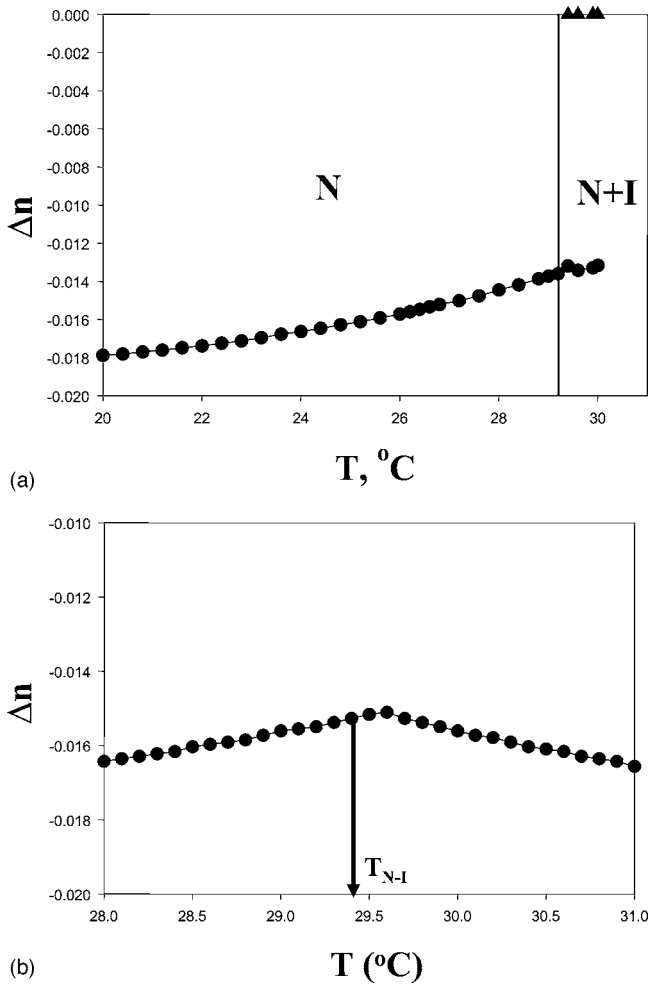

FIG. 10. $\Delta n(T)$ of DSCG, $c=15$ wt % for two wavelengths $\lambda=633$ (a) and 546 nm (b), respectively. Circles correspond to the *N* phase, triangles to the *I* phase. Points above the *N*-*I* phase transition were obtained for the nematic and isotropic parts of the biphasic region using a pinhole.

sated by the portion of the wedge in which the optical retardation is about 300 nm, i.e., $\Delta n \approx -0.02$. Using interference filters and the quartz wedge, we measured Δn for the solution with $c=13$ wt % at four different wavelengths. The data are represented by open circles in Fig. 9(b) and agree well with the data measured by the spectroscopic technique for other concentrations. We estimate the accuracy of the Δn value to be about ± 0.001.

The temperature dependence $\Delta n(T)$ for $c=15$ wt %, obtained from the microspectrophotometer data, are shown in Figs. 10(a) and 10(b) for two wavelengths, $\lambda=633$ and 546 nm, respectively. Experimental points in the biphasic region correspond to the *N* phase coexisting with the islands of the *I* phase. To select the region of measurements, we inserted an opaque screen with a calibrated pinhole that allowed us to analyze the texture in a circular spot of about 10 μm diameter. Note that the absolute value $|\Delta n|$ of the *N* phase might increase with temperature in the biphasic region, as clearly seen in Fig. 10(b). The reason is that the *N* phase in the biphasic region becomes more concentrated, as discussed in the next section.

b. Blue 27: Birefringence and Absorption. Blue 27 is a light absorbing material. The transmitted intensity for an absorbing crystal plate with its optical axis oriented at the angle α with respect to two parallel polarizers is of the form [64]

$$t = \left(t_0 \cos^4\alpha + t_{90} \sin^4\alpha + \frac{\sqrt{t_0 t_{90}}}{2} \cos\Delta\varphi \sin^2 2\alpha \right) \quad (2)$$

where $\Delta\varphi = 2\pi\Delta n d/\lambda$ (as in the case of transparent materials) and $t_0 = \exp(-4\pi k_\parallel d/\lambda)$ and $t_{90} = \exp(-4\pi k_\perp d/\lambda)$ are the transmittances at $\alpha=0$ and 90°, respectively. We use the transmission spectra $t_0(\lambda)$ and $t_{90}(\lambda)$ to determine the absorption indices $k_\parallel$ and $k_\perp$ for light with polarization parallel and perpendicular to the director, respectively. To determine $\Delta\varphi$ and Δn, one needs an additional measurement at α different from 0 and 90°. As follows from Eq. (2), the best accuracy is achieved for $\alpha=45°$. We thus calculate $\Delta\varphi$ and Δn by additionally measuring the transmittance t_{45} at $\alpha=45°$ and using the formula

$$\cos\Delta\varphi = \frac{4t_{45} - (t_0 + t_{90})}{2\sqrt{t_0 t_{90}}}. \quad (3)$$

The two equations above allow one to measure simultaneously birefringence, absorption, and absorption anisotropy.

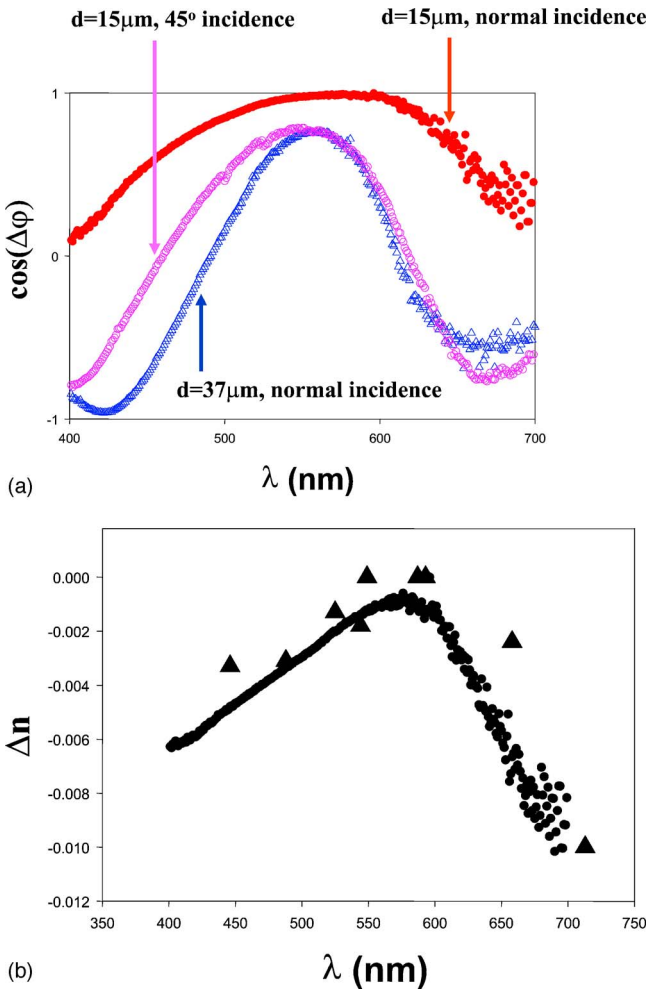

FIG. 11. (Color online) Birefringence of 4.5 wt % Blue 27: (a) $\cos\Delta\varphi$ vs λ, for $d=15$ μm at normal (solid circles) and 45° (empty squares) incidence and for $d=37$ μm at normal incidence; (b) birefringence measured with the quartz wedge for several wavelengths (triangles); dispersion of the birefringence for 4.5 wt % of Blue 27 in water ($T=20$ °C) obtained from (a) and Eq. (3) (solid circles).

To determine Δn from the spectroscopic data, we plotted $\cos\Delta\varphi$ in Eq. (3) as a function of λ for a planar Blue 27 cell of thickness $d=15$ μm and normal light incidence [Fig. 11(a)]. Note that Eq. (3) allows one to determine the phase retardation with the uncertainty of $2\pi m$, where m is an integer number. To determine m, we prepared a planar wedge cell with the director perpendicular to the thickness gradient. A Mylar spacer of thickness 75 μm was placed parallel to the rubbing direction at one side of the wedge; the thin side had no spacer. The wedge demonstrated only one set of interference colors somewhat modified by the dichroism of the material. It allowed us to conclude that $m=0$ as for $m\geqslant 1$ one would observe multiple sets of interference colors.

The values of Δn were first determined from the spectroscopic data. The dependency $\cos\Delta\varphi$ vs λ was measured for $d=15$ μm at normal [Fig. 11(a), solid circles] and 45° incidence [Fig. 11(a), open squares]; in addition, it was measured for a thicker cell, $d=37$ μm, at normal incidence [Fig. 11(a), open triangles]. The dependencies $\cos\Delta\varphi$ vs λ are rather unusual as compared to similar plots in regular materials, in which Δn depends only slightly on λ. In our case, $\cos\Delta\varphi$ vs λ plots often feature maxima with amplitude less than 1 [Fig. 11(a)]. This behavior can be attributed to the fact that near the maxima, in addition to $\Delta\varphi\approx 0$ and $m=0$, the function $\Delta n(\lambda)$ is nonmonotonic, approaching almost zero values near $\lambda=575$ nm. The dispersion of birefringence $\Delta n(\lambda)$ for 4.5 wt % Blue 27, calculated using Eq. (3) and the data for $d=15$ μm and normal incidence and shown in Fig. 11(b), is clearly nonmonotonic; Δn is negative and approaches almost a zero value ($\Delta n\approx -0.001\pm 0.001$) near $\lambda=575$ nm.

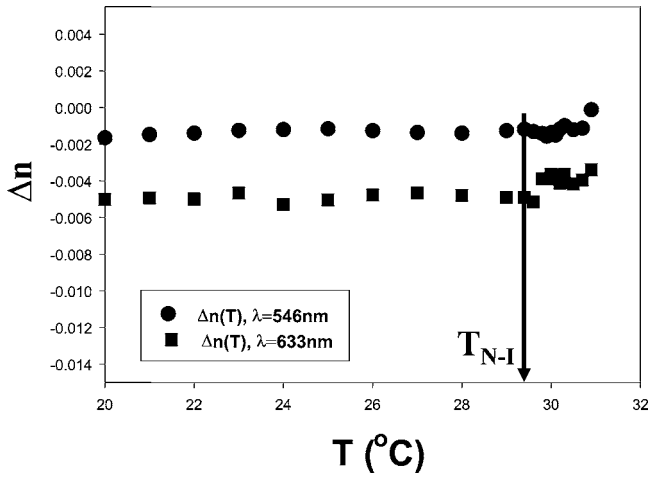

FIG. 12. Temperature dependencies of birefringence of 4.5 wt % Blue 27 solution measured at two different wavelengths $\lambda=633$ (filled circles) and 546 nm (filled squares).

To verify whether Δn remains negative and does not change its sign near $\lambda=575$ nm, we used the quartz wedge. The cell of thickness 15 μm filled with 4.5 wt % Blue 27 solution was tested under the polarizing microscope in a monochromatic mode with a quartz wedge. The optic axis of the wedge was perpendicular to the director $\hat{\mathbf{n}}$. From the shift of the extinction bands of first order we determined that Δn remains negative and measured its value for several wavelengths [filled triangles in Fig. 11(b)].

Figure 12 shows the temperature dependencies of Δn for 4.5 wt % Blue 27 solution measured at $\lambda=633$ (filled circles) and 546 nm (filled squares).

Absorption spectra were calculated from the transmission data, measured for a planar nematic Blue 27 cell with $d=5$ μm and $\alpha=0$ and 90°, at two different temperatures, 20 and 27 °C (Fig. 13). The temperature dependencies of $k_{\parallel}$ and $k_{\perp}$ measured at $\lambda=633$ nm (which is close to the maximum of the absorption band for Blue 27) are shown in Fig. 14. These data will be used in the next section to determine the scalar order parameter S.

c. Violet 20: Birefringence and Absorption. The absorption anisotropy and birefringence for Violet 20 (5 wt % aqueous solution), Fig. 15, have been determined as in the case of Blue 27. As in Blue 27, Δn and $\Delta k=k_{\parallel}-k_{\perp}$ are both negative; the dispersion of Δn is nonmonotonic, as in the Blue 27 case.

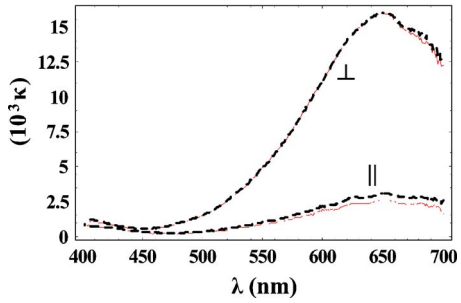

FIG. 13. (Color online) Spectra of the absorption coefficients for 4.5 wt % Blue 27, recalculated from the transmission data measured for a planar *N* cell for parallel and perpendicular polarizations of the incident light with respect to the director for $T=20$ (solid lines) and 27 °C (dashed lines).

4. Order parameter measurements

The absorption anisotropy (linear dichroism) can be used to deduce the nematic scalar order parameter S (see for example [56,57]):

$$S = \frac{2(gN-1)}{(gN+2)(3\cos^2\beta - 1)}, \tag{4}$$

where $N=k_{\|}/k_{\perp}$ is the dichroic ratio, β is the angle between the molecular symmetry axis and the dipole moment of the transition that is responsible for absorption, and g is a correction factor accounting for the anisotropy of refractive indices and local field (exciton) effects. Analysis based on the Green's function formalism [58] shows that S can be recovered more properly from the ratio of the integral absorption moments $M_{\|(\perp)}$ rather than from the dichroic ratio at a single wavelength. Thus the formula (4) holds but with the integrated dichroic ratio determined as $N=N_M=M_{\|}/M_{\perp}$, where $M_{\|}$ and $M_{\perp}$ are the integral absorption moments for the polarizations parallel and perpendicular to the director, respectively:

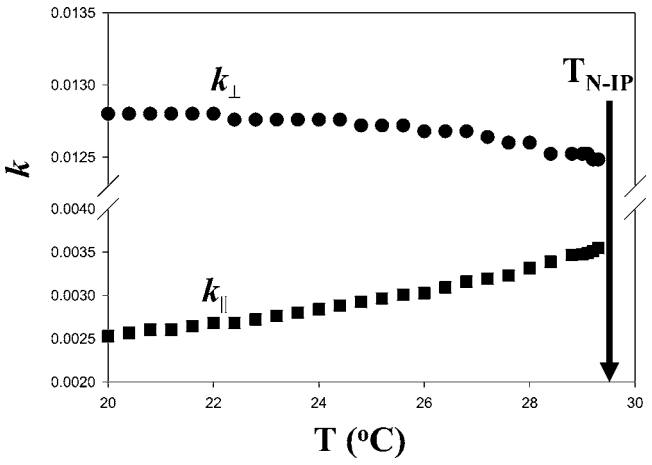

FIG. 14. The temperature dependencies of $k_{\|}$ and $k_{\perp}$ for 4.5 wt % Blue 27 measured at $\lambda=633$ nm.

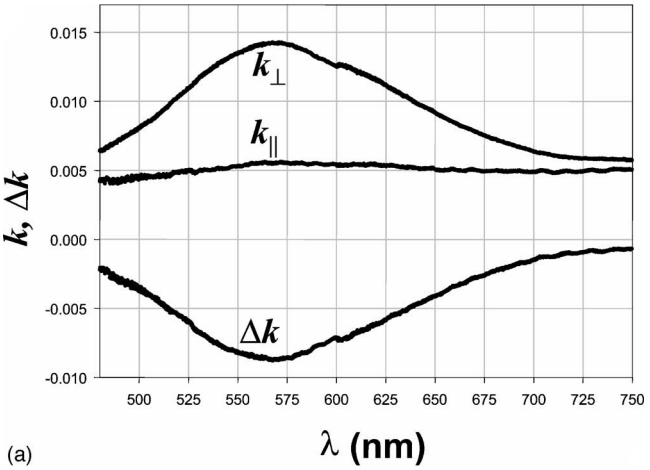

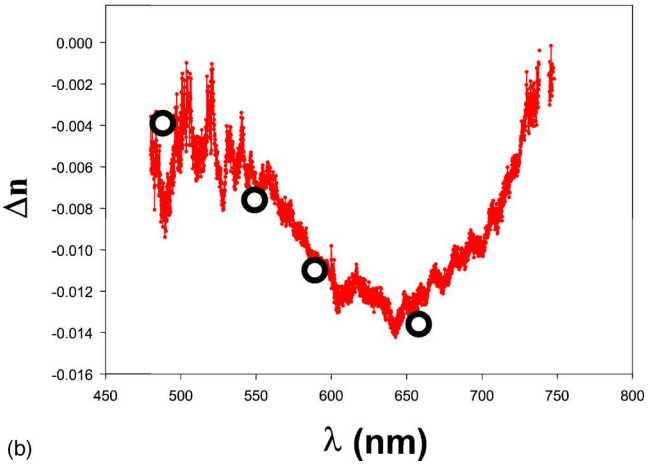

FIG. 15. (Color online) Absorption spectra (a) and dispersion of the birefringence (b) for 5 wt % Violet 20, calculated from the transmission data measured for a planar nematic cell: absorption coefficient $k_{\|}$ corresponds to $\hat{n}\|\hat{P}$ ($\hat{P}$ is the direction of the incident light polarization) whereas $k_{\perp}$ corresponds to $\hat{n}\perp\hat{P}$ and $\Delta k=k_{\|}-k_{\perp}$; open circles in (b) correspond to the data obtained with the quartz wedge.

$$M_{\|(\perp)} = \int \mathrm{Im}(\varepsilon_{\|(\perp)})d\omega = 2\int n_{\|(\perp)}\kappa_{\|(\perp)}d\omega. \tag{5}$$

The integration is performed over the frequency region of the absorption band; the correction factor g is also modified, $g=g_M$. The calculation of S from the standard dichroic ratio $N=k_{\|}/k_{\perp}$ is valid only when the absorption bands have the same shape for two orthogonal polarizations and when the dispersion of refractive indices within the absorption band is small. If these conditions are satisfied, the standard and the integral approach match each other, provided one takes into account the relationship between the two correction factors, $g=g_M n_{\|}/n_{\perp}$.

The effect of orientational order on the spectral properties of LCLCs is different as compared to the case for thermotropic LCs, because an individual molecule of a LCLC finds itself in the environment of the aggregate. On the other hand, the birefringence of LCLCs is rather small, so $g_M \approx 1$. As a

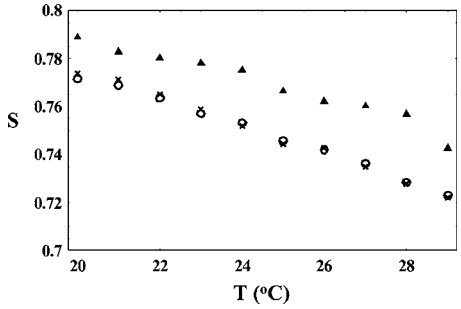

FIG. 16. Temperature dependencies of the order parameter of 4.5 wt % Blue 27 determined (1) by integrating Eq. (5) through the accessible range of the absorption band 480–700 nm (crosses); (2) by approximating the absorption bands with Gaussian peaks (solid triangles); (3) from the ratio of amplitudes of the absorption peaks for two orthogonal polarizations (open circles).

result, the integral absorption moments in the N phase can be expressed through the individual integral absorption moments $M^C_{\parallel(\perp)}$ of a column that is parallel (perpendicular) to the director:

$$M_{\parallel} = \frac{C_c}{3}[(2S+1)M^C_{\parallel} + 2(1-S)M^C_{\perp}],$$

$$M_{\perp} = \frac{C_c}{3}[(2+S)M^C_{\perp} + (1-S)M^C_{\parallel}], \tag{6}$$

where C_c is the column concentration. The values of C_c is difficult to determine without knowing how many molecules form an aggregate. Fortunately, C_c drops out of the expression for S:

$$S = \frac{1+\alpha_M/2}{1-\alpha_M}\frac{1-N_M}{1+N_M/2}. \tag{7}$$

Here $\alpha_M = M^C_{\parallel}/M^C_{\perp}$ is an integral dichroic ratio of the LCLC aggregate that depends on the orientation of the dipole transition moment with respect to the aggregate axis. For Blue 27 the dipole transition moment is in the plane of the molecule. Furthermore, the molecular planes are apparently perpendicular to the aggregate axis. The latter is supported by (1) simulations of the mutual orientation of molecular pairs using SPARTAN software and (2) measurements of the dichroic ratio for a dry film of Blue 27 well aligned when doped with a block copolymer additive as described in Ref. [26]; the measurement yields a very low value $N<0.05$. Therefore, one can simplify the consideration by putting $M^C_{\parallel}=0$ and Eq. (7) reduces to

$$S = \frac{1-N_M}{1+N_M/2}. \tag{8}$$

Figure 13 shows that the absorption band extends beyond the long-wave limit of the spectral region accessible for measurements. Therefore we use three methods to calculate S (Fig. 16). First, we estimate N_M by integrating (5) through the accessible range of absorption band (480–700 nm); the corresponding values of S are represented with crosses. In the second technique, we approximate the absorption bands with Gaussian peaks and determine N_M and S (solid triangles) from this fitting. In the third approach, we follow the approximate but widely used procedure and estimate N_M as the ratio of amplitudes of the absorption peaks for two orthogonal polarizations, the corresponding values of S are represented with open circles. Figure 16 shows that the Gaussian approximation method yields values of S somewhat higher than the other two. Although we can offer a possible explanation of this fact (associated with the redshift of the absorption peak for the polarization parallel to the transition dipoles as compared to the peak for the orthogonal polarization, an effect similar to the Davydov splitting in molecular crystals [59]), the difference in the values of S is not significant, only about 0.03.

III. DISCUSSION

A. Absorption spectra

It is well known that molecular aggregation results in spectroscopic changes such as shifts of the maxima of absorption bands [61,62], and resonance light scattering [6], caused by changes in molecular interactions. Our data above suggest that there is no visible shift in the positions of absorption bands, at least in the concentration range studied (above $c=10^{-4}$ wt % and $c_M=2$ μM), which also implies that aggregation most probably takes place at lower concentration. And indeed, the very recent data on fluorescence of DSCG [63] indicate that the fraction of molecules bound into aggregates increases when concentration rises above $c=10^{-6}$ wt % ($c_M=20$ nM).

We therefore conclude that in the studied range of concentrations the molecules are already aggregated; of course, the aggregates might coexist with some number of individual molecules.

B. Birefringence

The optical characterization procedure described in Sec. II B 3 to characterize the anisotropic absorption and birefringence of LCLCs is based on the approach developed for absorbing crystals [64]. The approach is justified when the LCLC is well aligned within the area probed by the light beam.

The measured Δn are small (from about −0.02 for DSCG to about −0.001 or less for Blue 27 and Violet 20) which is natural as these aqueous solutions are highly diluted. These data are not influenced much by the nonzero birefringence of the buffed polymer layers used to align the LCLC. The thickness of the LCLC layers (10–100 μm) in all the experiments was orders of magnitude larger than the thickness of the polymer layers (100 nm). Direct measurements show that the optical retardation caused by the buffed polyimide aligning layers is of the order of 2 nm [65]. The optical retardation caused by the birefringence of LCLCs in cells of thickness 15 μm is significantly larger, ranging from 300 nm for DSCG to the lowest value of 15 nm as measured for Blue 27 in the spectral region 550–600 nm [Fig. 11(b)]. Therefore, the finite birefringence of polyimide layers is lower than the

accuracy of our Δn measurements, ±0.001. The data for the *I* phase (Fig. 10) also support this conclusion.

The birefringence of Blue 27 $c=4.5$ wt % solution is much smaller than that for DSCG at $c=15$ wt %. The feature of almost zero birefringence of Blue 27 near $\lambda=575$ nm can be attributed to the effect of the absorption band and anomalous dispersion. For the Blue 27 solutions, absorption is most efficient for polarization in the plane of the molecules, i.e., perpendicular to the director. Therefore, one should expect that the ordinary refractive index $n_o=n_\perp$ (the subscript refers to polarization perpendicular to the director) would reach a minimum at a wavelength that is somewhat shorter than the maximum of the absorption band (650 nm). The extraordinary index of refraction $n_e=n_\parallel$ should not experience this dispersion effect as the absorption along the director is much weaker (Fig. 13). This difference in the behavior of n_o and n_e explains the nonmonotonic $\Delta n(\lambda)$ with a minimum near $\lambda=575$ nm that is somewhat smaller than the absorption maximum of Blue 27 at 650 nm. In this spectral region, Blue 27 can be considered as a dichroic but nonbirefringent LCLC. A similar nonmonotonic $\Delta n(\lambda)$ trend is observed in the absorbing solutions of Violet 20 (Fig. 15).

In lyotropic LCs formed by molecular aggregates there might be at least two mechanisms for birefringence. The first is caused by the molecular anisotropy, while the second one, the so-called form birefringence [66,67], is caused by the anisotropy of molecular aggregates. The interplay between the molecular anisotropy and form birefringence was documented by Nallet and Barois [66] for the surfactant lamellar L_α phase in which the rodlike molecules (positive Δn) are arranged into lamellae (negative Δn) [66,68]; the two contributions can cancel each other at a particular wavelength, which depends on composition.

In the *N* phase of the studied LCLC materials, we have the opposite situation: the planklike LCLC molecules (negative Δn) are stacked into rods (positive Δn). In our case, Δn remains negative (although small) in the studied spectral range, i.e., the form birefringence is not as significant as the molecular anisotropy contribution to the total birefringence.

The wide biphasic region allows one to determine Δn in the *N* phase in coexistence with the *I* phase (Figs. 10 and 12). The *N* phase is more concentrated than the *I* phase, which is verified by direct observation of the biphasic sample in a test tube: the *I* part is floating above the higher-density *N* phase. The increase of $|\Delta n|$ with *T* observed in the biphasic region suggests that the corresponding *N* phase is more concentrated not only as compared to the *I* phase but also as compared to the *N* phase at temperatures just below the biphasic region; therefore, its order parameter and $|\Delta n|$ might be higher. This conclusion is supported by the enhancement of deuteron quadrupole splitting observed by Yu and Saupe [69] in the *N* part of the biphasic region for DSCG in D_2O; the latter result means that *S* increases in the biphasic region.

C. Absorption anisotropy and scalar order parameter

Both Blue 27 and Violet 20 in the *N* phase show negative absorption anisotropy around the absorption band with the maximum approximately at $\lambda=650$ (Fig. 13) and 570 nm [Fig. 15(a)], respectively: light polarized parallel to the molecular plane is absorbed most strongly. The *N* phase of both materials is uniaxial, as verified in the experiments with cells tilted with respect to the incident light by an angle up to 60°: within the accuracy of the experiment, the values for Δk and Δn and the positions of the absorption maxima remained the same in the spectral region 400–700 nm.

The anisotropy of absorption allowed us to determine the scalar order parameter for the *N* phase of Blue 27 and its temperature dependence (Fig. 16). The data clearly demonstrate a decrease in *S* as the system approaches the *N-I* transition; this decrease is small, about 5%–7% over the range of about 10 °C. At the transition point, $S_c=0.73\pm0.01$.

The measured values of *S* are much higher that those in the regular thermotropic nematic liquid crystals and in the Maier-Saupe theory (in which $S_c=0.43$) [70], but are close to the predictions of the Onsager theory ($S_c=0.84$) for the *N* phase formed by rigid rods [60].

The Onsager model has been developed to describe the occurrence of orientational order in a system of thin long rods. The rods are supposed to be rigid and not interacting with each other (except through the effect of "excluded volume"). Above some concentration that depends on the length-to-diameter ratio $L/D\gg1$, the system phase separates into a more concentrated and ordered *N* phase and a less concentrated *I* phase.

The Onsager model predicts a high value of the order parameter in the *N* phase, as compared to the values found in typical thermotropic low-molecular-weight nematic materials. The original result based on the trial function produced $S=S_c=0.84$ [60]. More accurate (numerical) solutions resulted in somewhat lower values [71,72], $S=S_c=0.79$, very close to our results. The Onsager model describes satisfactorily many polymer liquid crystalline systems, since in these systems it is easy to achieve the condition $L/D>10$ for which the accuracy of solution is acceptable. The LCLCs seem to satisfy the condition $L/D>10$, even in the *I* phase close to the *I-N* transition, as follows from the light scattering data taken at temperatures just above the *N-I* transition [8].

Despite a close match between the Onsager model and the data above, the correspondence is not complete. The most obvious difference is that the Onsager model predicts no temperature dependence of *S*. The experimentally observed decrease of *S* with temperature can be considered as the evidence of aggregate interactions (other than pure steric excluded volume repulsion) and/or the effect of temperature dependence of the aggregate length [8]. As the aggregates are formed by molecules with ionic groups at the periphery (that make them water soluble), multibody Coulomb interactions (aggregate-aggregate, aggregate-counterions, and counterions-counterions) might play an important role in stability and ordering of LCLCs, as suggested by a number of recent models developed for similar systems such as polyelectrolytes [13,73–75]. The length polydispersity of LCLC aggregates [37,41,76] and their finite flexibility should also be taken into account in the description of LCLCs.

As already indicated, the scalar order parameter for water solutions of DSCG has been estimated by Goldfarb *et al.* to range from 0.76 in 4 wt % solution (at low temperatures) to

0.97 in 29 wt % solution (which probably corresponded to the *M* phase) [34]. Lower values of the order parameter have been observed recently by Horowitz *et al.* [10] in the LCLC material Sunset Yellow FCF: S decreases from $S=0.76$ at room temperature to about $S_c=0.6$ at the *N-I* transition ($\approx 72\,^{\circ}$C). The difference in the values of S_c measured for Blue 27 and Sunset Yellow FCF might be attributed to a much larger temperature interval of the *N* phase in the latter material.

IV. CONCLUSION

We have characterized the optical properties of the *N* phase formed by aqueous solutions of three different materials: DSCG, Blue 27, and Violet 20. The individual molecules in all these materials have a planklike shape and assemble into rodlike aggregates. According to the light absorption anisotropy data, the molecular planes are on average perpendicular to the aggregate axes and thus to the nematic director, indicating thus the *H*-type aggregation. The x-ray diffraction data demonstrate a pronounced peak that corresponds to 0.34 nm spacing along the director, which is consistent with the idea of a stack with face-to-face molecular assembly. We did not find any evidence of strong changes in the aggregation features for concentrations above 10^{-4} wt %$(2\ \mu M)$; apparently, the molecules are already aggregated at these concentrations. At low concentrations, the molar absorption coefficient decreases as the concentration of the LCLC molecules increases. Once the concentration reaches 4–10 wt % $(0.1M)$ at room temperature, one observes formation of the optically uniaxial *N* phase.

By achieving a good alignment of the LCLCs in cells with buffed polyimide layers, we have determined the birefringence of these materials in the nematic and biphasic regions and found it to be negative and significantly lower in absolute value as compared to the birefringence of the typical thermotropic *N* materials. In the absorbing materials Blue 27 and Violet 20, the wavelength dependence $\Delta n(\lambda)$ is nonmonotonic, which can be attributed to the effect of anomalous dispersion near the absorption bands.

We have observed and described positive and negative tactoids that represent elongated cusped inclusions of one phase into another in the biphasic *N-I* region (which is wide in all three materials studied). The director field within the tactoids shows bend and splay deformations but no twist; it remains tangential to the curved *N-I* interface.

Finally, we determined the scalar order parameter of the *N* phase of Blue 27 and found it to be relatively high and weakly temperature dependent, which puts the findings into the domain of general validity of the Onsager model.

LCLCs are an interesting representative of a broad family of materials with a one-dimensional molecular self-assembly. They are similar to living polymers, solutions of rodlike viruses, wormlike micelles, polyelectrolyte solutions, etc. Their unique optical properties and the possibility to prepare well-aligned monodomain samples might allow one to perform a broader range of experimental studies as compared to other systems and to test a number of interesting phenomena, such as the role of electrostatic interactions in the formation of orientationally ordered phases. Further studies are needed to determine phase diagrams and other properties of LCLCs as a function of the ionic content of the solutions, aggregation number, etc.

ACKNOWLEDGMENTS

This research was partially supported by NSF/ITIC Grant No. DMR0346348, CRDF Award No. UKP1-2617-KV-04, and STCU Grant No. 3091, and by the National Academy of Science of Ukraine (Grant No. 1.4.1B/109). We thank P. J. Collings for discussions and for sending us the manuscript [10] before publication. We thank K. Antion, C. Bailey, A. Golovin, and R. Twieg for useful discussions and suggestions.

[1] J. Lydon, in *Handbook of Liquid Crystals*, edited by D. Demus, J. Goodby, G. W. Gray, H.-W. Spiess, and V. Vill (Wiley-VCH, Weinheim, 1998), Vol. 2B, pp. 981–1007, and references therein.
[2] J. Lydon, Curr. Opin. Colloid Interface Sci. **3**, 458 (1998); **8**, 480 (2004).
[3] A. S. Vasilevskaya, E. V. Generalova, and A. S. Sonin, Russ. Chem. Rev. **58**, 904 (1989).
[4] *J-Aggregates*, edited by T. Kobayashi (World Scientific, Singapore, 1996).
[5] W. J. Harrison, D. L. Mateer, and G. T. Tiddy, J. Phys. Chem. **100**, 2310 (1996).
[6] R. F. Pasternack and P. J. Collings, Science **269**, 935 (1995).
[7] P. Camorani, M. Furier, O. Kachkovskii, Yu. Piryatinskiy, Yu. Slominskiy, and V. Nazarenko, Semicond. Phys., Quantum Electron. Optoelectron. **4**, 229 (2001).
[8] Yu. A. Nastishin, H. Liu, S. V. Shiyanovskii, O. D. Lavrentovich, A. F. Kostko, and M. A. Anisimov, Phys. Rev. E **70**, 051706 (2004).
[9] P. K. Maiti, Y. Lansac, M. A. Glaser, and N. A. Clark, Liq. Cryst. **29**, 619 (2002).
[10] V. R. Horowitz, L. A. Janowitz, A. L. Modic, P. A. Heiney, and P. J. Collings, Phys. Rev. E **72**, 041710 (2005).
[11] *Micelles, Membranes, Microemulsions, and Monolayers*, edited by W. M. Gelbart, A. Ben-Shauk, and D. Roux (Springer-Verlag, New York, 1994).
[12] J. T. Kindt and W. M. Gelbart, J. Chem. Phys. **114**, 1432 (2001).
[13] I. I. Potemkin, R. E. Limberger, A. N. Kudlay, and A. R. Khokhlov, Phys. Rev. E **66**, 011802 (2002).
[14] F. A. Escobedo, J. Chem. Phys. **118**, 10262 (2003).
[15] K. Ghosh and M. Muthukumar, Phys. Rev. Lett. **91**, 158303 (2003).
[16] J. F. Dreyer and C. W. Ertel, J. Phys. Colloid Chem. **52**, 808 (1948).
[17] T. Sergan, T. Schneider, J. Kelly, and O. D. Lavrentovich, Liq.

Cryst. **27**, 567 (2000).
[18] Y. Bobrov, C. Cobb, P. Lazarev, P. Bos, D. Bryant, and H. Wonderly, SID Int. Symp. Digest Tech. Papers **31**, 1102 (2000).
[19] W. C. Wip, H. S. Kwok, V. M. Kozenkov, and V. G. Chigrinov, Displays **22**, 27 (2001).
[20] R. C. Advincula, E. Fells, and M.-K. Park, Chem. Mater. **13**, 2870 (2001).
[21] S.-W. Tam-Chang, W. Seo, I. K. Iverson, and S. M. Casey, Angew. Chem., Int. Ed. **42**, 897 (2003).
[22] C. Ruslim, M. Hashimoto, D. Matsunaga, T. Tamaki, and K. Ichimura, Langmuir **20**, 95 (2004).
[23] I. G. Khan, S. V. Belyaev, N. V. Malimonenko, V. F. Kleptsyn, M. L. Kukushkina, N. N. Masanova, V. V. Solovei, and G. N. Vorozhtsov, SID Int. Symp. Digest Tech. Papers **35**, 1316 (2004).
[24] Y. Bobrov, O. Kuchenkova, M. Kouznetsov, P. Lazarev, A. Manko, V. Nazarov, N. Ovchinnikova, M. Paukshto, P. Protsenko, and S. Remizov, J. Soc. Inf. Disp. **12**(2), 125 (2004).
[25] Y. Ukai, T. Ohyama, L. Fennell, Y. Kato, M. Paukshto, P. Smith, O. Yamashita, and S. Nakanishi, SID Int. Symp. Digest Tech. Papers **35**, 1170 (2004).
[26] T. Schneider, A. Golovin, J.-C. Lee, and O. D. Lavrentovich, J. Inf. Display, Korean Inf. Display Soc. **5**(2), 27 (2004).
[27] M. D. Lavrentovich, T. Sergan, and J. R. Kelly, Liq. Cryst. **30**, 285 (2003).
[28] S. V. Shiyanovskii, T. Schneider, I. I. Smalyukh, T. Ishikawa, G. D. Niehaus, K. J. Doane, C. J. Woolverton, and O. D. Lavrentovich, Phys. Rev. E **71**, 020702(R) (2005).
[29] T. Schneider, K. Artyushkova, J. E. Fulghum, L. Broadwater, A. Smith, and O. D. Lavrentovich, Langmuir **21**, 2300 (2005).
[30] O. D. Lavrentovich and T. Ishikawa, U.S. Patent No. 6,411,354 (2002); U.S. Patent No. 6,570,632 (2003).
[31] J. S. G. Cox, G. D. Woodard, and W. C. McCrone, J. Pharm. Sci. **60**, 1458 (1971).
[32] N. H. Hartshorne and G. D. Woodard, Mol. Cryst. Liq. Cryst. **23**, 343 (1973).
[33] D. Perahia, D. Goldfarb, and Z. Luz, Mol. Cryst. Liq. Cryst. **108**, 107 (1984).
[34] D. Goldfarb, Z. Luz, N. Spielnerg, and H. Zimmermann, Mol. Cryst. Liq. Cryst. **126**, 225 (1985).
[35] K. Ichimura, T. Fujiwara, M. Momose, and D. Matsunaga, J. Mater. Chem. **12**, 3380 (2002).
[36] T. Fujiwara and K. Ichimura, J. Mater. Chem. **12**, 3387 (2002).
[37] T. J. Sluckin, Liq. Cryst. **6**, 111 (1989).
[38] P. A. Buining and H. N. W. Lekkerkerker, J. Phys. Chem. **97**, 11510 (1993).
[39] R. M. L. Evans, Phys. Rev. E **59**, 3192 (1999).
[40] A. Speranza and P. Sollich, J. Chem. Phys. **117**, 5421 (2002).
[41] H. H. Wensink and G. J. Vroege, J. Chem. Phys. **119**, 6868 (2003)
[42] T. Schneider and O. D. Lavrentovich, Langmuir **16**, 5227 (2000)
[43] M. Kleman and O. D. Lavrentovich, *Soft Matter Physics: An Introduction* (Springer-Verlag New York, 2003), Chap. 13.
[44] J. D. Bernal and I. Fankuchen, J. Gen. Physiol. **25**, 111 (1941).
[45] J. X. Tang, R. Oldenbourg, P. G. Allen, and P. A. Janmey, in *Materials Science of the Cell*, edited by B. Mulder, V. Vogel, and C. Schmidt, MRS Symposia Proceedings No. 489 (Materials Research Society, Pittsburgh, 1998), p. 33.
[46] A. V. Kaznacheev, M. M. Bogdanov, and S. A. Taraskin, J. Exp. Theor. Phys. **95**, 57 (2002).
[47] P. Prinsen and P. van der Schoot, Phys. Rev. E **68**, 021701 (2003).
[48] A. V. Kaznacheev, M. M. Bogdanov, and A. S. Sonin, J. Exp. Theor. Phys. **97**, 1159 (2003).
[49] P. Prinsen and P. van der Schoot, J. Phys.: Condens. Matter **16**, 8835 (2004).
[50] S. V. Lishchuk and C. M. Care, Phys. Rev. E **70**, 011702 (2004).
[51] G. E. Volovik and O. D. Lavrentovich, Zh. Eksp. Teor. Fiz. **85**, 1997 (1983) [Sov. Phys. JETP **58**, 1159 (1984)].
[52] R. D. Williams, J. Phys. A **19**, 3211 (1986).
[53] R. Ondris-Crawford, E. P. Boyko, B. G. Wagner, J. H. Erdmann, S. Zumer, and J. W. Doane, J. Appl. Phys. **69**, 6380 (1991).
[54] T. Schneider, Ph.D. dissertation, Chemical Physics Interdisciplinary Program, Kent State University, Kent, OH, 2005 (unpublished).
[55] B. K. Ganguly and P. Bagchi, J. Org. Chem. **21**, 1415 (1956)
[56] L. M. Blinov, *Electro-Optical and Magneto-Optical Properties of Liquid Crystals* (Wiley, New York, 1983).
[57] B. Bahadur, in *Handbook of Liquid Crystals*, edited by D. Demus (Wiley-VCH, Weinheim, 1998), Vol. 2A, p. 257.
[58] V. I. Sugakov and S. V. Shiyanovskii, Opt. Spektrosk. **48**, 542 (1980) [Opt. Spectrosc. **48**, 298 (1980)].
[59] V. I. Sugakov and S. V. Shiyanovskii, Fiz. Tverd. Tela (Leningrad) **22**, 901 (1980) [Sov. Phys. Solid State **22**, 527 (1980)].
[60] L. Onsager, Ann. N.Y. Acad. Sci. **51**, 627 (1949)
[61] E. E. Jelley, Nature (London) **138**, 1009 (1936); **139**, 631 (1937);
[62] G. Scheibe, L. Kandler, and H. Ecker, Naturwiss. **25**, 75 (1937)
[63] R. Vasyuta, O. Boiko, Yu. Piryatinskiy, V. Nazarenko, and A. Kachkovskii, Mol. Cryst. Liq. Cryst. **426**, 117 (2005).
[64] A. F. Konstantinova, B. N. Grechushnikov, B. V. Bokut, and Ye. G. Valyashko, *Optical Properties of Crystals* (Navuka i Teknnika, Minsk, 1995) (in Russian).
[65] Yu. A. Nastishin, R. D. Polak, S. V. Shiyanovskii, V. H. Bodnar, and O. D. Lavrentovich, J. Appl. Phys. **86**, 4199 (1999).
[66] P. Barois and F. Nallete, J. Phys. II **4**, 1049 (1994).
[67] M. Born and E. Wolf, *Principles of Optics*, 7th ed. (Cambridge University Press, Cambridge, U.K., 1999)
[68] J. Rogers and P. A. Winsor, Nature (London) **216**, 477 (1967).
[69] L. J. Yu and A. Saupe, Mol. Cryst. Liq. Cryst. **80**, 129 (1982).
[70] P. G. de Gennes and J. Prost, *The Physics of Liquid Crystals*, 2nd ed. (Clarendon Press, Oxford, 1993).
[71] A. N. Beris and B. J. Edwards, *Thermodynamics of Flowing Systems* (Oxford Science Publications, New York, 1994), Chap. 11.
[72] S.-D. Lee and R. B. Meyer, J. Chem. Phys. **84**, 3443 (1986).
[73] S. B. Chen and D. L. Koch, J. Chem. Phys. **104**, 359 (1996).
[74] K. Ghosh, G. A. Carri, and M. Muthukumar, J. Chem. Phys. **116**, 5299 (2002).
[75] I. I. Potemkin and A. R. Khokhlov, J. Chem. Phys. **120**, 10848 (2004).
[76] A. Speranza and P. Sollich, Phys. Rev. E **67**, 061702 (2003).